ASSESSMENT OF NON LINEAR BOND LAWS FOR NSM SYSTEMS IN CONCRETE ELEMENTS

Francesca CERONI
Assistant Professor
University of Sannio
Benevento, Italy
*ceroni@unisannio.it**

Joaquim BARROS
Full Professor
University of Minho
Guimarães, Portugal
barros@civil.uminho.pt

Marisa PECCE
Full Professor
University of Sannio
Benevento, Italy
pecce@unisannio.it

Marco IANNICIELLO
Master in Civil Engineering
University of Sannio
Benevento, Italy
marcoianniciello@libero.it

Abstract

In this paper the numerical FEM model developed to simulate the behaviour of the NSM strengthening system for concrete elements is presented. The plane model introduces the non linear bond law of the system by an interface element between the composite reinforcement and the concrete considered linear. The results of two experimental programs are analysed and used to calibrate the parameters of the bond shear-slip relationship by means the numerical model. The procedure is based on the inverse analysis of the experimental data in order to have the better fitting of the global pull-out load-displacement curves.

Keywords: Bond-slip law, FEM model, NSM technique

1. Introduction

Over the last years, the use of fibre reinforced polymer (FRP) materials for repair and strengthening of concrete structures has progressively increased, due to the several advantages related to these composites when compared to the steel [1] [2].

In the last decades, a strengthening technique designated by near surface mounted (NSM) has been proposed to increase the flexural and shear strength of RC members precluding the debonging failure. NSM systems are composed by FRP rods and strips that are installed into pre-cut grooves open on the concrete cover of the element to be strengthened [3] [4]. Several researches have studied the NSM technique, performing experimental tests to characterize both the load-carrying capacity and the bond strength of these systems [5] [6] [7] [8]. The experimental results evidence that the load-carrying capacity of NSM systems is strongly influenced by the bond performance, which is strictly dependent of the material, surface configuration and type of the FRP reinforcement.

The objective of this research is to derive a bond stress-slip relationship, $\tau - s$, for the modelling of the bond behaviour between NSM FRP bars/strips and concrete by using a finite element approach (FEM). Using the $\tau - s$ proposed by Sena Cruz and Barros [7], the bond behaviour of several specimens tested by Bilotta et al. [9] and Macedo et al. [10] were simulated by performing FEM analysis in order to derive the values of parameters of the bond law that assure the best fitting of the force-end slip relationship obtained experimentally. Some of the results are presented herein.

2. Experimental results

2.1 Experimental programs

The results of two experimental programs of bond tests on various types of NSM systems carried out by the Authors using different types of tests set-up have been considered in this
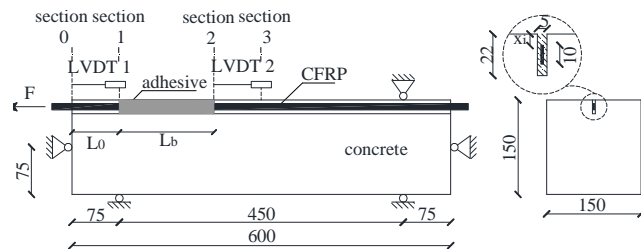
paper. The meaningful data of both programs, discussed in detail in [9] [10], are summarized in the following and individuated as program 1 and 2.

The specimens of program 1 tested in [9] are made of prismatic concrete blocks (dimensions $b_c = 160$ mm, $h_c = 200$ mm, $L_c = 400$ mm) strengthened with FRP bars or strips bonded according to the NSM technique (Figure 1). Three bond tests have been performed on equal specimen for each FRP typology; in particular, 6 different types of bar/strips have been embedded into a groove longitudinally cut in the cover of the prisms after concrete hardening (Figure 1). The same bond length was used for all the specimens ($L_b = 300$ mm).

Five strain gauges 70 mm spaced have been glued on the NSM surface before applying the adhesive.
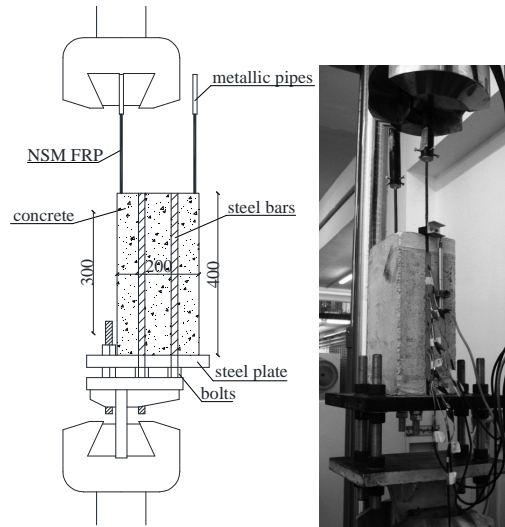
Figure 1. Set-up of experimental program 1.   **Figure 2. Set-up of experimental program 2.**

The main test variables were: type of reinforcement (bars or strips), type of fibers (glass, basalt, carbon), Young's modulus (46-182 GPa), bars diameter ($d = 6$-8-10 mm). Furthermore, the bars have different surface treatment: sand coated round basalt bars with diameter 6 and 8 mm (B-6-SC and B-8-SC), ribbed round glass bars with ribs cut in the hardened bars with diameter 8 mm (G-8-RB), smooth round carbon bars with diameter 8 mm (C-8-S), and smooth carbon strips with thickness 2.5 mm and width 15 mm (C-2.5x15-S). The round bars were introduced into square grooves of 10 and 14 mm edge for the bars of 6 and 8 mm diameter, respectively and, thus, the shape ratio k is defined as ratio of groove edge to-bar diameter; by contrast, the strip was introduced into a rectangular groove of 25 mm x 8 mm cross section, and k is defined as ratio of groove-tostrip width. The values of k, are always greater than 1.5, which is the minimum value suggested to avoid the splitting failure of the epoxy [8]. Epoxy adhesive was used to bond the bars and the strips into the grooves.

All specimens have been cast in the same batch; the mean cylindrical compressive strength at 28 days after the casting was $f_{cm} = 19$ MPa and the mean Young's modulus was 18.6 GPa.

In the experimental program 2 carried out by Macedo et al. [10] the pull-out configuration represented in Figure 2 was used. Prismatic concrete specimens with dimensions of 150x150x600 mm^3 were adopted and several bond lengths were analyzed. The depth and width of the groove was 22 mm and 5 mm, respectively. One displacement transducer (LDTV1) was used to measure the displacement between the left edge of concrete specimen (*section 0*) and the first FRP point bonded to concrete (*section 1*); in the following it will be referred as displacement at loaded end, d_l. A second displacement transducer (LDTV2) was used to register the displacement at free end, d_{fr}, by measuring the displacement between the

last FRP bonded point (*section 2*) and the concrete point located at *section 3*. Strain gauges glued to the CFRP were used to estimate the strain variation in the bonded region.

To assess the influence on the system performance of the bond length and the depth at which the CFRP strip is located into the groove, 10 pullout tests were performed using 5 different values of bond length, L_b; therefore for each couple of specimens with same L_b, 2 different positions of the strip into the groove, x_i, were considered (Figure 2). The generic denomination of series is LbY_xZ, where Y and Z are the CFRP bond length (40, 70, 90, 120 and 150 mm) and its position in the groove (6 and 12 mm), respectively. To evaluate the concrete properties, three compressive tests on cylinder specimens at 28 days after casting were performed and gave a mean value of 25.0 MPa and 29.0 GPa for the compressive strength, f_{cm}, and Young's modulus, E_c, respectively.

2.2 Experimental results

For each NSM system of programs 1 and 2, Tables 1 and 2 include the following relevant results: ultimate tensile strength f_{fu}, Young's modulus E_f, axial stiffness $E_f A_f$, groove shape factor k, failure mode, maximum load F_{max}, and the loaded end slip at F_{max}, d_{max}. The mechanical properties of FRP indicated in these tables are the average values obtained by experimental tensile tests on five specimens according to [11]. In program 1 the displacements d were calculated by integrating the strains measured along the bonded length, while in program 2 they were obtained by the difference between the LVDT1 measure, d_l, and the elastic elongation of the unbounded part of the FRP strip.

Table 1. Main experimental data and results for program 1.

Specimen	f_{fu} [MPa]	E_f [GPa]	$E_f A_f$ [kN]	K [-]	Failure mode[a]	F_{max} [kN]	d_{max} [mm]
B-6-SC-1	1282	46	1300	1.67	E/C	33.87	2.93
B-6-SC-2					E/C	28.84	2.37
B-8-SC-1	1272	46	2311	1.75	E/C	31.57	1.08
B-8-SC-2					E/C	33.10	0.86
B-8-SC-3					E/C	30.24	1.45
G-8-RB-1	1333	59	2964	1.75	E/C	46.71	2.50
G-8-RB-2					E/C	45.25	1.51
G-8-RB-3					E/C	50.86	2.15
C-8-S-1	2495	155	7787	1.75	E/C+CL	48.52	0.88
C-8-S-2					E/C+CL	55.30	1.10
C-8-S-3					E/C+CL	45.23	0.84
C-2.5x15-S-1	2863	182	6825	1.67	E/C	52.97	1.32
C-2.5x15-S-2					E/C	56.03	1.28
C-2.5x15-S-3					E/C	46.26	1.24

[a] E/C: debonding at the epoxy-concrete interface, CL: detachment of a concrete layer

Table 2. Main experimental data and results for program 2.

Specimen	f_{fu} [MPa]	E_f [GPa]	$E_f A_f$ [kN]	K [-]	Failure mode[a]	F_{max} [kN]	d_{max} [mm]
Lb40_x6	2879	156	2184	2.20	S	18.59	0.60
Lb40_x12					S	19.90	0.41
Lb70_x6	2879	156	2184	2.20	S	27.69	0.68
Lb70_x12					S	31.43	0.64
Lb90_x6	2879	156	2184	2.20	S	33.90	0.92
Lb90_x12					S	35.63	0.82
Lb120_x6	2879	156	2184	2.20	S	34.46	0.72
Lb120_x12					S	37.92	0.79
Lb150_x6	2879	156	2184	2.20	S	36.43	1.03
Lb150_x12					S	38.35	0.85

[a] S: Splitting of adhesive

3. The numerical analysis

3.1 The FEM model

The numerical simulations were carried out with *FEMIX v4.0* FEM-based computer program [12]. To simulate the boundary conditions of the test specimens of program 1, in the FEM model (Figure 3a) the inferior part of the specimen was restrained with supports, prescribing the displacement in direction 3 (Figure 3b). The test was modeled as a plane stress problem. Due to structural symmetry conditions only half part of specimen was considered.

Four-node Lagrangian plane stress elements with a 2x2 Gauss-Legendre integration scheme were used to simulate the concrete and the CFRP strip; the thickness of 200 mm and 15 mm were assigned for the concrete and CFRP, respectively. The adhesive was simulated by four-node line finite interface elements with two-point Lobatto integration rule. The tangential stiffness of these interface elements is defined once the parameters that define the local τ - s law are known. In regard to the normal stiffness, a constant value of 1.0e+06 N/mm^3 is considered.

The CFRP strip and concrete were modeled as linear elastic materials, considering the Young modulus values determined in the experimental tests, and a Poisson coefficient of 0.0 and 0.2 for the CFRP and concrete, respectively.

The load was applied in two points, and the arc-length method was used with the controlling displacement at loaded end of CFRP, by applying a displacement increment of 0.01 mm in direction 3 (Figure 3b).
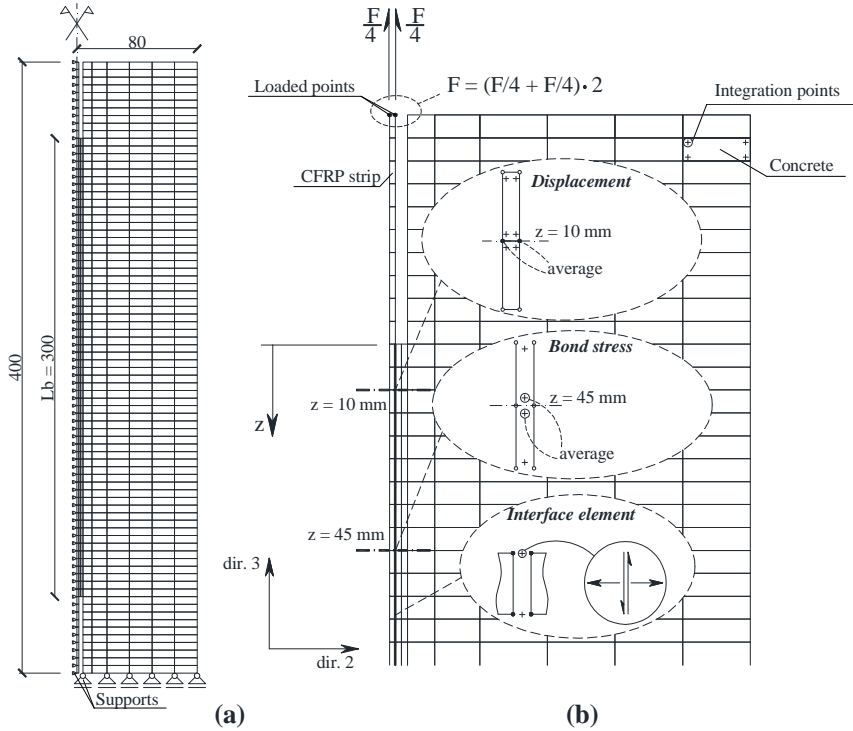

Figure 3. Finite element idealization of C-2.5x15-S series: (a) complete mesh; (b) zoom on the top side.

3.2 The bond law of the interface element

In the present work the determination of the local bond stress-slip relationship for both strips and bars is based on the approach from [7]. The non linear bond law, $\tau - s$, can be defined as follows:

$$\tau(s) = m_{lin} \cdot s \qquad\qquad \tau(s) = \tau_{max}\left(\frac{s}{s_{max}}\right)^{\alpha} \qquad\qquad\qquad \tau(s) = \tau_{max}\left(\frac{s}{s_{max}}\right)^{-\alpha'} \qquad (1)$$

$$\text{if } s \le s_{lim} \qquad\qquad \text{if } s_{lim} \le s \le s_{max} \qquad\qquad \text{if } s > s_{max}$$

where τ_{max} is the shear strength and s_{max} its corresponding slip, respectively, α and α' are parameters defining the shape of the curves and m_{lin} is the initial stiffness of the bond law (Figure 4a). The softening branch of the bond law can tend asymptotically towards a residual or a zero shear stress. The trends of the influence of the characteristics of a local bond-stress-slip law on the pull-out behavior of a specimen in a bond test (represented by the pull-out force-displacement relationship, F - d) are represented in Figure 4b.
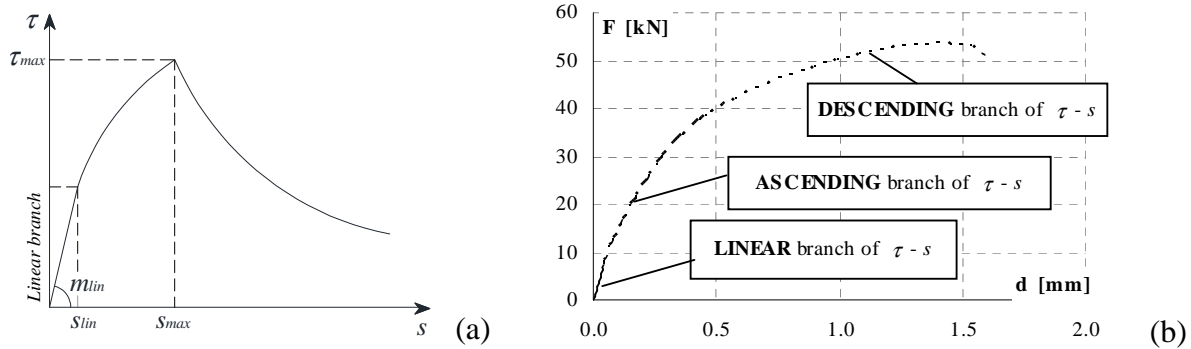

Figure 4. (a) Local bond stress-slip relationship; (b) qualitative correlation between τ-s and F-d relationships in a bond test.

3.3 The influence of bond law parameters on the pull out load

The bond law depends on five parameters, but the following ones have relevant influence on the bond behaviour:

- the peak value of bond stress-slip curve, τ_{max}, and its corresponding slip, s_{max};
- the parameter that defines the shape of the post-peak branch of $\tau-s$ relationship, α'.

Each one has a different impact on the strength of the system, as showed in Figure 5. In this graphic the parameter ξ is given by the following expression:

$$\xi = \frac{s_{max}}{s_{max}^0} = \frac{\tau_{max}}{\tau_{max}^0} = \frac{\alpha'}{\alpha'^0} \qquad (2)$$

where s_{max}^0, τ_{max}^0 and α'^0 represent the minimum values of s_{max}, τ_{max} and α' used in the parametric studies, respectively (i.e. $s_{max}^0 = 0.08$mm, $\tau_{max}^0 = 1.25$MPa and $\alpha'^0 = 0.20$).
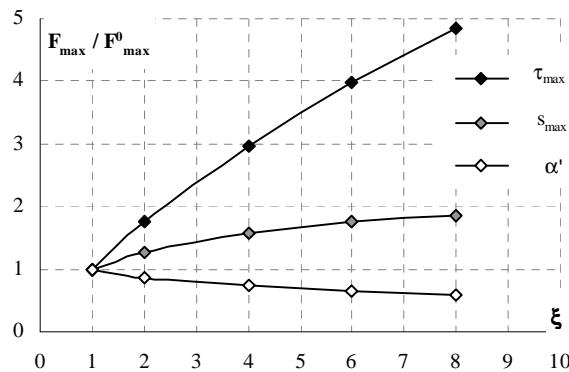

Figure 5. Evaluation of the impact of s_{max}, τ_{max} and α' on the F_{max}.

F_{max}^0 is the maximum pullout force when using these values.

Figure 5 shows that the parameter that most affects the maximum pull-out force value is the local bond peak stress, τ_{max}; in fact, when $\xi = 8$, the ratio F_{max} / F_{max}^0 is about 5.

4. Experimental-numerical comparison

4.1 The inverse analysis

The differential equation of bond was solved for some of the specimens tested in [9] [10] assuming the bond law given by Eq. (1). The first assessment of the bond law parameters for specimens of program 1 was tried using the experimental $\tau - s$ relationships obtained by means the strain gauges measurements. In particular, the shear stress was calculated by using the measures of the first two strain gauges placed at 10 and 80 mm from the beginning of FRP bonded length and, thus, the experimental measures refer to the abscissa $z = 45$ mm. The corresponding slip was calculated by integrating the experimental measures of strain along the bond length.

However, the results were not satisfactory when the force-displacement curves, $F - d$, were numerically determined and compared with the experimental ones. Therefore, an inverse analysis based on the comparison of the experimental pull-out force-displacement curves, $F - d$, with the numerical ones, was performed to assess the two parameters s_{max} and α', while the τ_{max}, s_{lim} and α were fixed by considering the local experimental bond law. The parameter s_{ult} is defined when the maximum pull-out force is attained.

In Table 3 the values of the parameters are listed for each NSM system together with the theoretical and the mean experimental failure load. In Figures 6 the whole numerical and experimental $F - d$ curves are compared. A good compliance can be observed both in terms of $F - d$ curves and of maximum load. The values of the parameters of the bond law are those that assure the best fitting of the average $F - d$ curve of the three specimens that compose each series.

Finally, in Figures 7 the $\tau - s$ bond law derived from the strain gauges measures, and the one determined from inverse analysis addressed to the optimization of the curve $F - d$ are compared for two experimental cases. The shear stress is evaluated by considering the perimeter at the concrete-resin interface for the specimens of program 1 (failure at the concrete-resin interface) and the perimeter at the reinforcement-resin interface for specimens of program 2 (splitting failure). The graphs evidence a quite good predictive performance up to bond strength, and a significant deviation between both approaches in the $\tau - s$ descending branch. This deviation could be due to the larger uncertainness of the experimental measures when the bond law attains the post-peak branch.

Table 3. Main parameters of the bond laws assessed by inverse analyses.

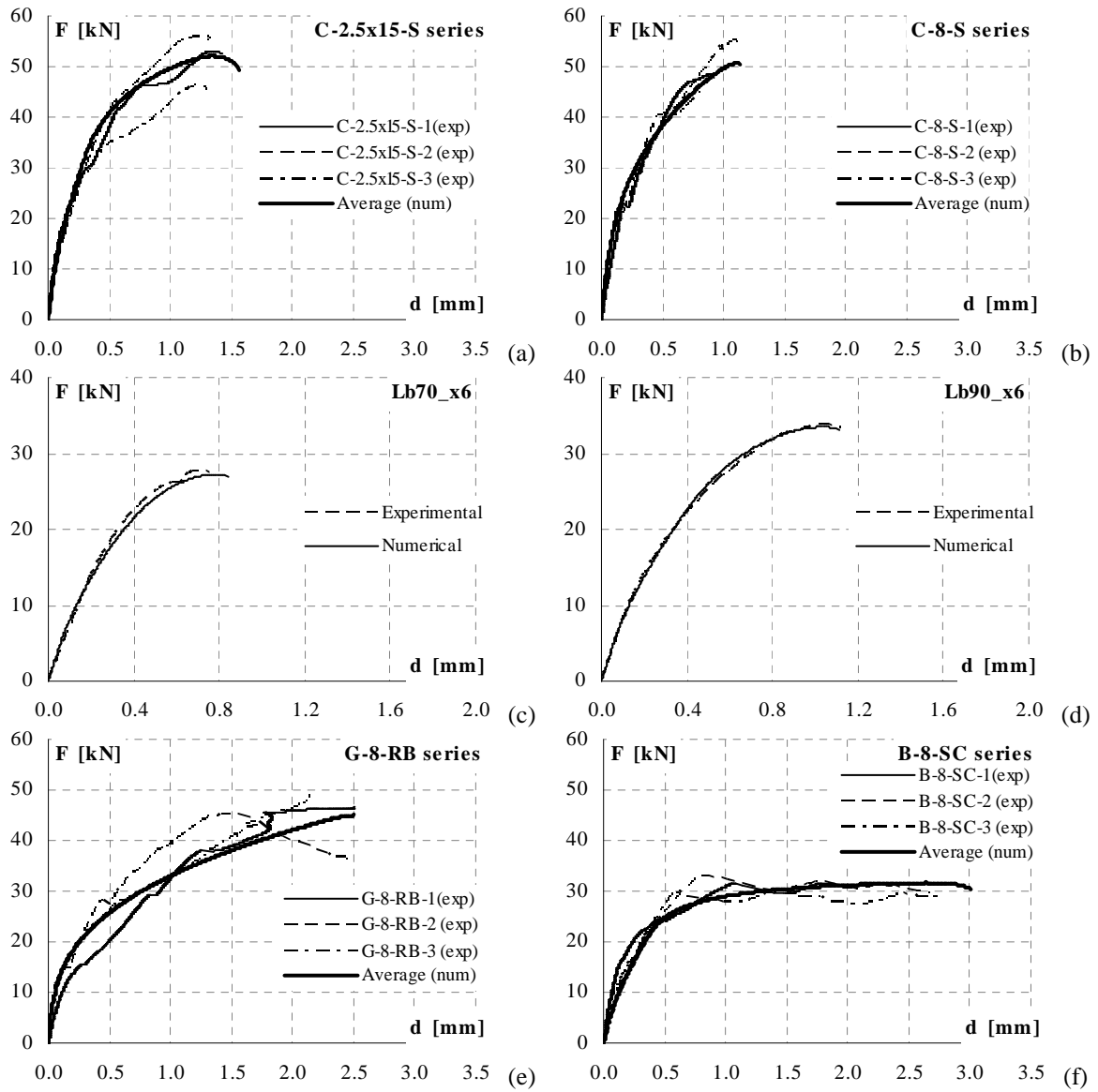| Specimen	E_f [GPa]	s_{lin} [mm]	s_{max} [mm]	τ_{max} [MPa]	α [-]	α' [-]	s_{ult} [mm]	$F_{max,th}$ [kN]	$F_{max,exp}$ [kN]
B-6-SC	46	0.05	0.41	7.09	0.40	0.65	2.30	29.21	29.17
B-8-SC	46	0.05	0.43	7.63	0.40	1.93	2.51	31.67	31.59
G-8-RB	59	0.01	0.08	6.50	0.40	0.32	2.42	45.01	47.06
C-8-S	155	0.01	0.10	5.73	0.40	0.31	0.92	50.62	49.61
C-2.5x15-S	159	0.05	0.33	5.26	0.35	1.13	1.32	52.05	51.75
Lb70_x6	156	0.05	0.40	8.70	0.40	0.40	0.84	27.27	27.69
Lb90_x6	156	0.05	0.40	8.70	0.40	0.40	1.11	33.50	33.90

Figure 6. Experimental vs. theoretical pull-out force-displacement curves for different NSM systems: (a) carbon strips 2.5 mm x 15 mm; (b) carbon bars 8 mm; (c) carbon strips 1.4 mm x 10 mm; (d) carbon strips 1.4 mm x 10 mm; (e) ribbed glass bars 8 mm; (f) sand coated basalt bars 8 mm.
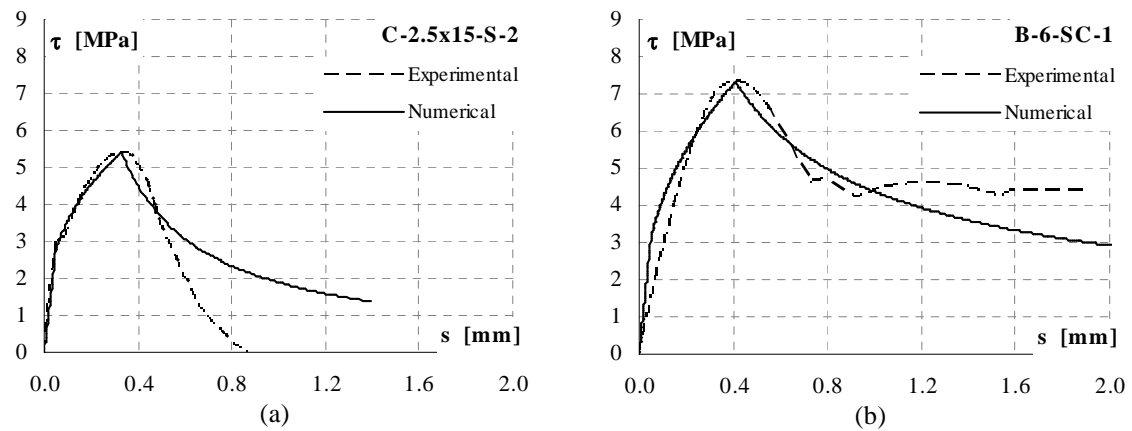

Figure 7. Numerical-experimental comparisons of the local bond-law: (a) carbon strips 2.5 mm x 15 mm; (b) basalt bars 6 mm.

5. Conclusions

The FEM modelling applied to the technique of NSM strengthening appears efficient to calibrate the parameters of the selected type of bond law. The results of the calibration point out the global reliability of the shape of the $\tau - s$ relationship in terms of simulating the pull-out load-displacement curve.

The potentiality of the developed model allows to analyse and to compare the behaviour of the various types of FRP elements in terms of maximum local shear stress and its corresponding slip, bond length effect, stress field and concrete crack pattern.

References

[1] ACI-440, "Guide for design and construction of externally bonded FRP systems for strengthening concrete structures", *ACI Technical Report,* May 2002, 118 pp.

[2] CEB-FIB, "Externally bonded FRP reinforcement for RC structures", *International Federation for Structural Concrete - Technical report,* July 2001, 130 pp.

[3] BLASCHKO, M., ZILCH, K., "Rehabilitation of concrete structures with CFRP strips glued into slits", *Proceeding of the 12th International Conference on Composite Materials,* Paris, France, July 1999.

[4] DE LORENZIS, L., NANNI, A., LA TEGOLA, A., "Strengthening of reinforced concrete structures with near surface mounted FRP rods", *Proceeding of the International meeting on composite materials - PLAST,* Milan, Italy, May 2000, 8 pp.

[5] DE LORENZIS, L., NANNI, A., "Shear strengthening of reinforced concrete beams with near-surface mounted fiber reinforced polymer rods", *ACI Structural Journal,* Vol. 98, No. 1, January/February 2001, pp. 60-68.

[6] HASSAN, T., RIZKALLA, S., "Investigation of bond in concrete structures strengthened with near surface mounted carbon fiber reinforced polymer strips", *ASCE Journal of Composites for Construction,* Vol. 7, No. 3, August 2003, pp. 248-257.

[7] SENA CRUZ, J.M., BARROS, J.A:O., "Bond Between Near-Surface Mounted Carbon-Fiber-Reinforced Polymers Laminate Strips and Concrete", *ASCE Journal of Composite for Construction,* Vol. 8, No. 6, November/December 2004, pp. 519-527.

[8] DE LORENZIS, L., TENG, J.C., "Near-surface mounted FRP reinforcement: An emerging technique for strengthening structures", *Composites Part B: Engineering,* Vol. 38, March 2007, pp. 119-43.

[9] BILOTTA, A., CERONI, F., DI LUDOVICO, M., NIGRO, E., PECCE, M., MANFREDI, G., "Bond efficiency of EBR and NSM FRP systems for strengthening of concrete members", *ASCE Journal of Composites for Construction,* published on line, doi: 10.1061/(ASCE)CC.1943-5614.0000204.

[10] MACEDO, L., COSTA, I.G., BARROS, J.A.O., "Avaliação da influência das propriedades de adesivos e da geometria de laminados de fibra de carbono no comportamento de ensaios de arranque (Evaluation of influence of adhesive and geometry of laminated carbon fiber on the behavior of startup tests)", *Proceeding of Betão Estrutural 2008,* Guimarães, Portugal, November 2008 [in Portuguese].

[11] ASTM-D3039, "Specification for Concrete Aggregates", *ASTM International,* West Conshohocken, PA, 2003, doi: 10.1520/C0033-03, URL: http://www.astm.org.

[12] SENA CRUZ, J.M., BARROS, J.A:O., "Numerical simulation of the nonlinear behavior of RC beams strengthened with NSM CFRP strips", *Proceedings of Congress on numerical methods in engineering*, Porto, Portugal, June 2007, 20 pp.